PHYSICAL REVIEW B **95**, 165133 (2017)

Internal field effect on vortex states in the layered organic superconductor λ-$(BETS)_2Fe_{1-x}Ga_xCl_4$ ($x = 0.37$)

S. Uji
National Institute for Materials Science, Tsukuba, Ibaraki 305-0003, Japan
and Graduate School of Pure and Applied Sciences, University of Tsukuba, Tsukuba, Ibaraki 305-8577, Japan

T. Terashima, T. Konoike, and T. Yamaguchi
National Institute for Materials Science, Tsukuba, Ibaraki 305-0003, Japan

S. Yasuzuka
Research Center for Condensed Matter Physics, Hiroshima Institute of Technology, Saeki, Hiroshima 731-5193, Japan

A. Kobayashi and B. Zhou
Department of Humanities and Sciences, Nihon University, Setagaya, Tokyo 156-8550, Japan
(Received 2 February 2017; published 24 April 2017)

Resistance and magnetic torque measurements have been performed to investigate an internal field effect on vortex states for a layered organic superconductor λ-$(BETS)_2Fe_{1-x}Ga_xCl_4$ ($x = 0.37$), where BETS = bis(ethylenedithio)tetraselenafulvalene. Because of the internal field by the localized $3d$ spins of the Fe ions, the superconducting transition temperature has a maximum at 14 T. The strongest energy dissipation due to Josephson vortex dynamics and the largest pinning of pancake vortices are observed at ∼14 T. The interlayer resistance in parallel fields shows a characteristic dip with decreasing temperature. The dip temperature decreases with increasing field, suggesting a Josephson vortex transition. At ∼23 T, we observe another small dip in the field dependence of the interlayer resistance, steep deceases of the perpendicular critical field, and diamagnetism. These results show a phase transition of the superconductivity, which is likely ascribed to an inhomogeneous superconducting transition.

DOI: 10.1103/PhysRevB.95.165133

I. INTRODUCTION

The two-dimensional (2D) organic conductors λ-$(BETS)_2MCl_4$ (M = Fe, Ga), where BETS is bis(ethylenedithio) tetraselenafulvalene, are known to show unique phase diagrams [1–3]. At zero magnetic field, λ-$(BETS)_2FeCl_4$ shows a metal-insulator (MI) transition at ∼8 K (T_{MI}), which is associated with an antiferromagnetic order [3,4]. This antiferromagnetic insulating (AFI) phase is removed by applying a field of about 10 T, and then a paramagnetic metallic (PM) phase is restored [3,5]. When a magnetic field is applied parallel to the conducting planes (ac plane), superconducting (SC) phase is induced above 17 T and then destroyed above 42 T at low temperatures [6,7]. This field-induced superconducting (FISC) phase does not appear in fields perpendicular to the conducting layers. The observations of the Shubnikov–de Haas and angular dependent magnetoresistance oscillations [8] reveal the 2D character of its Fermi surface in close agreement with band calculations [1]. The FISC phase is qualitatively understood in terms of Jaccarino-Peter (JP) effect [9,10], where the antiferromagnetic interaction $J_{\pi-d}$ between the π spin in the BETS layer and $3d$ spin in the $FeCl_4$ anion, the so-called $\pi - d$ interaction, plays a crucial role. At low temperatures and high fields, the internal field $H_{\rm int}$ made by the $3d$ spins is about 32 T, giving the highest transition temperature ($T_c \simeq 4$ K) of the FISC phase at 32 T [8,11]. In contrast, the isostructural nonmagnetic salt λ-$(BETS)_2GaCl_4$, which has a similar Fermi surface, remains metallic and shows a SC transition at $T_c \simeq 6$ K [12,13].

In the alloys, λ-$(BETS)_2Fe_xGa_{1-x}Cl_4$, the AFI phase shrinks as x decreases [14]. Since the average of $H_{\rm int}$ is reduced by the nonmagnetic Ga substitution, the FISC phase shifts to a low field region as x decreases. For $x \simeq 0.4$, the low and high field SC phases merge into a single SC phase as depicted in Fig. 1(a). Because of this $T_c(H)$ curve, the free energy $F_\pi(H)$ of the superconducting state relative to the normal state will have a form shown in Fig. 1(b); $F_\pi(H)$ has a minimum at the field where T_c has a maximum. The magnetization $M_\pi(H) = -dF_\pi/dH$ is depicted in Fig. 1(c). Here we should note that the $F_\pi(H)$ and $M_\pi(H)$ curves do not include the contribution of the $3d$ spins. An interesting feature is that the positive magnetization, $M_\pi(H) > 0$, appears even in the SC phase. The dotted lines indicate the complete magnetic-flux penetration, $M_\pi = 0$; the external field is completely canceled out by the internal field $H_{\rm int}$ by the $3d$ spins. For this JP system, the local current $j(r)$ in the SC state is calculated in the framework of the Ginzburg-Landau (GL) theory [15],

$$j_{\rm total}(r) = j_s(r) + j_p(r), \tag{1}$$

$$j_s(r) = \frac{e}{im}\{\Psi^*(r)\nabla\Psi(r) - \Psi(r)\nabla\Psi^*(r)\} - \frac{4e^2}{m}|\Psi(r)|^2 A(r), \tag{2}$$

$$j_p(r) = -2\mu_B\nabla\times(H - H_J)\left(1 - \frac{dH_J}{dH}\right)|\Psi(r)|^2, \tag{3}$$

 ©2017 American Physical Society

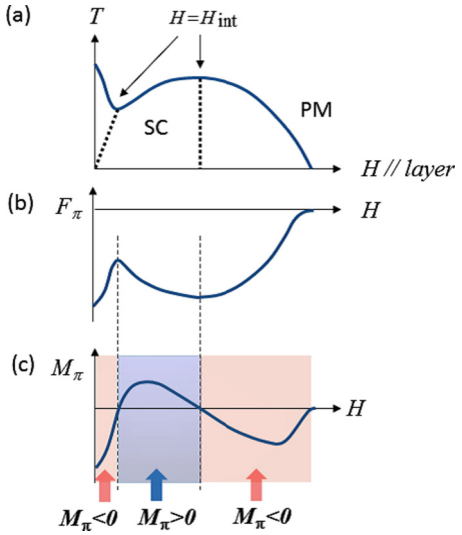

FIG. 1. (a) Schematic of the phase diagram of λ-$(BETS)_2Fe_xGa_{1-x}Cl_4$ for $x \simeq 0.4$. The dotted lines show the complete flux penetration, $M_\pi = 0$. (b) Free energy $F_\pi(H)$ of the electronic state at 0 K, which is expected from the phase diagram shown in (a). (c) Magnetization given by $M_\pi(H) = -dF_\pi/dH$.

where $j_s(r)$ is the supercurrent around the vortices and at the sample edges, arising from the orbital effect, and $j_p(r)$ the current due to the spin polarization (Zeeman effect). The exchange field H_J created by the $3d$ spins is defined as

$$H_J = J_{\pi-d}\langle S_{3d}\rangle/g\mu_B \geqslant 0. \tag{4}$$

The internal field $H_{\rm int}$, which the π spins see, is given by $H_{\rm int} = H_J - 1/\eta$, where $\eta = 0.44\alpha/\lambda_{so}T_c$ in the unit of tesla^{-1}. The Maki parameter is written as $\alpha = \sqrt{2}H^*_{c2}/H^{\rm Pauli}_{c2}$ [15], where H^*_{c2} is the orbital critical field. In the 2D limit, we note $H_{\rm int} = H_J$ since $\eta \to \infty (H^*_{c2} \to \infty)$.

Similarly, the magnetization is given by

$$M_\pi(r) = -\frac{\Phi_0}{4\pi\lambda^2}\frac{4}{n_s}\left[1+\eta(H-H_J)\left(1-\frac{dH_J}{dH}\right)\right]|\Psi(r)|^2, \tag{5}$$

where Φ_0 is the flux quantum, λ the penetration depth, and n_s the superconducting electron density. In high fields, $dH_J/dH \simeq 0$, so we have $j_p = 0$ and $M_\pi = 0$ for $H = H_{\rm int}$. For λ-$(BETS)_2Fe_xGa_{1-x}Cl_4$, $H_{\rm int} \simeq H_J$ since η is 5–10 [14].

For the first FISC material, $Eu_xSn_{1-x}Mo_6S_8$ with $H_{\rm int} \simeq 13$ T, the magnetization was measured in fields up to 20 T, and then paramagnetic behavior was slightly observed for $H < H_{\rm int}$ in the FISC phase, in addition to a large paramagnetic signal arising from the Eu moments [15].

At fields where $M_\pi = 0$, the theory [15] predicts that no conventional vortices are present because of the complete flux penetration. In such cases, energy dissipation mechanism of vortices, how vortices are driven by current, is unclear. In addition, the magnetic torque behavior, which is sensitive to the diamagnetism by the superconductivity, is another open question. In order to investigate these interesting points, we have performed the interlayer resistance and magnetic torque measurements in a wide temperature and field range for λ-$(BETS)_2Fe_xGa_{1-x}Cl_4$ for $x = 0.37$. For $x = 0.37$, whose phase diagram looks like that given in Fig. 1(a), the critical field H_{c2} (∼25 T) is rather easily accessible with our magnet systems.

II. EXPERIMENTS

The needlelike single crystals of λ-$(BETS)_2Fe_{1-x}Ga_xCl_4$ ($x = 0.37$), elongating along the c axis, were prepared by electrochemical oxidation in an appropriate solvent [1]. Four gold wires ($\phi 10\,\mu$m) were attached to the samples by carbon paste. The sample voltage V was measured by a conventional four-probe ac technique with electric current I along the b^* axis, perpendicular to the conducting ac plane. The resistance shown here is defined as $R = V/I$. The magnetic torque was measured by a microcantilever technique. The typical sample sizes are $\sim 0.04 \times 0.1 \times 0.5$ mm^3 for the resistance measurements and $\sim 0.04 \times 0.1 \times 0.2$ mm^3 for the torque. The experiments were performed by using a ^{3}He cryostat mounted in a 20 T superconducting or 30 T resistive magnet at Tsukuba Magnet Laboratories, NIMS.

III. RESULTS

A. Resistance

Figure 2 presents the temperature dependence of the interlayer resistance $R(T)$ in fields parallel to the c axis

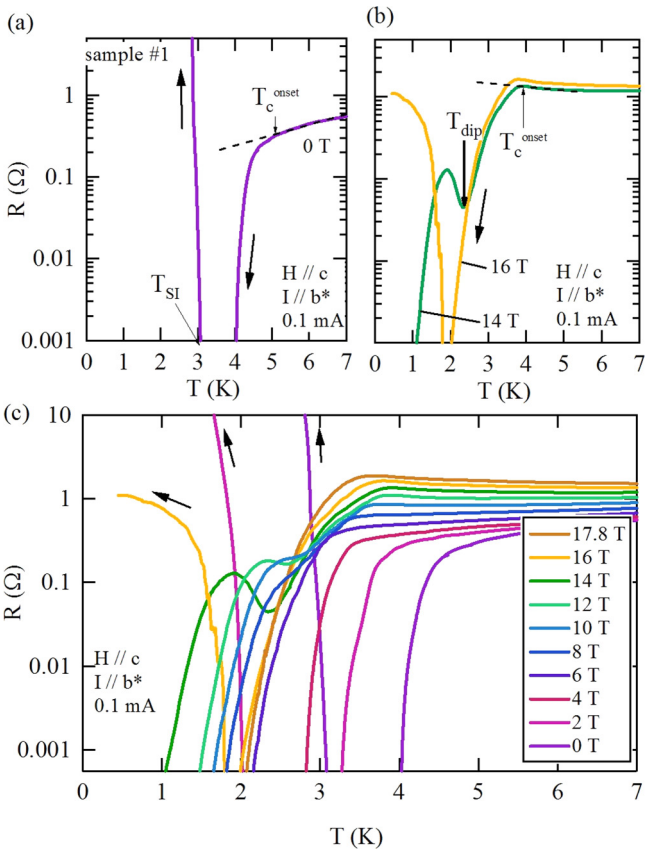

FIG. 2. Temperature dependence of the interlayer resistance $R(T)$ for sample no. 1 at (a) $\mu_B H = 0$ and (b) $\mu_B H = 14$ T and 16 T. (c) $R(T)$ curves at various fields. The current 0.1 mA corresponds to 0.5 A/cm^2.

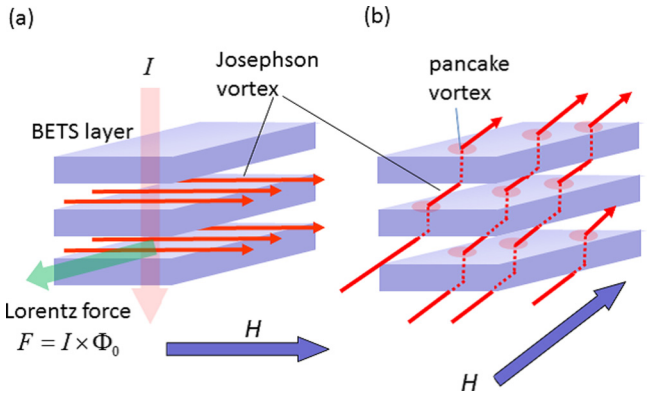

FIG. 3. Schematic pictures of flux lines in a layered superconductor. (a) In parallel fields, all the flux lines penetrate only in the insulating layers, forming JVs. A perpendicular current I drives the JVs in the layer direction. (b) In a tilted field, flux lines penetrate the SC layers, forming PVs.

($H \parallel$ layer). In zero field [Fig. 2(a)], the resistance decreases down to zero below 4 K and then quickly increases to a value higher than 10 kΩ below 3 K. These are the PM-SC and SC-AFI transitions, respectively [14]. Their transition temperatures, $T_c^{\rm onset}$ and $T_{\rm SI}$, are defined as shown in Fig. 2(a). At 14 T [Fig. 2(b)], the resistance has a broad maximum at $T_c^{\rm onset}$, and then decreases down to zero associated with a dip at 2.3 K ($T_{\rm dip}$). At 16 T, the resistance decreases to zero at 2 K, but rapidly comes back to a finite value at lower temperatures. The $R(T)$ curves at various fields are presented in Fig. 2(c).

In fields exactly parallel to the layers, all the flux lines penetrate only the insulating layers, forming Josephson vortices (JVs) [Fig. 3(a)]. JVs are weakly pinned in the insulating layers, where the order parameter vanishes. Therefore, a perpendicular current easily drives the JVs in the layer direction by Lorentz force. When the JVs, whose number is N_{JV}, are driven with a velocity $v_{\rm JV}$, a voltage $V \propto N_{\rm JV} v_{\rm JV} \Phi_0$ is induced; the driven JVs give rise to energy dissipation (finite resistance). As shown later, the finite resistance below $T_c^{\rm onset}$ in Fig. 2 can be ascribed to the JV dynamics. The dips in the $R(T)$ curves correspond to a relatively strong pinning of the JVs.

Figure 4(a) presents the $R(T)$ curves at various currents. At the lowest current, 0.075 mA, the resistance steeply decreases and then remains below the noise level below 2.2 K. At 0.085 mA, we observe finite resistance below 2 K, which can be ascribed to depinning of the JVs. As the current further increases, the dip behavior is suppressed. The dip at ~2 K shows a strong pinning of the JVs, whose origin will be discussed later. The dip temperature $T_{\rm dip}$ seems slightly current dependent. Figure 4(b) presents the $R(T)$ curves at various field angles. At $\theta = 0^\circ$ ($H \parallel c$), a dip is evident at ~2 K. As the field is tilted from the layer, the resistance in the low temperature region decreases and the dip becomes sharp. For $\theta > 0.5^\circ$, we observe a steep decrease and no dip. The results suggest that the flux lines penetrate the SC layers for $\theta > 0.5^\circ$, forming pancake vortices (PVs), and the flux lines are strongly pinned [Fig. 3(b)].

Figure 5 presents the interlayer resistance ($I \parallel b^*$) as a function of the field angle θ at 8 T. At the lowest current (0.025 mA), the resistance is below the noise level due to

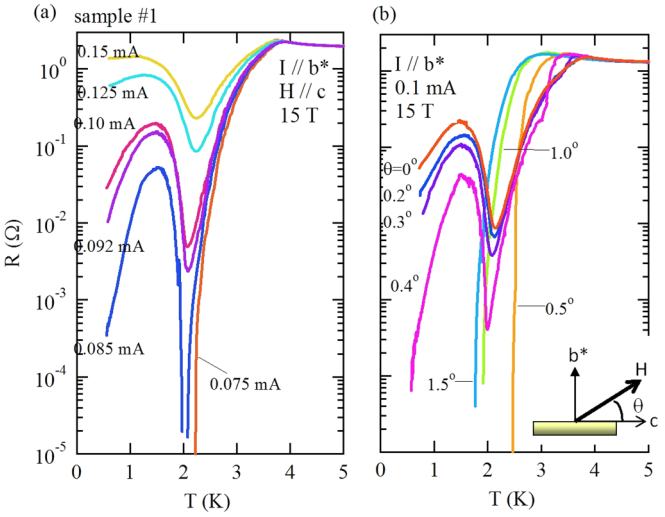

FIG. 4. Temperature dependence of the resistance $R(T)$ at various (a) currents and (b) field angles.

the SC transition when the field is nearly parallel to the c axis ($-1^\circ < \theta < 1^\circ$). As the current increases, the resistance increases, which is associated with a peak at $\theta = 0^\circ$ and side peaks (arrows) at $\theta = \pm 0.6^\circ$. At $\theta = 0^\circ$, the JVs are easily driven by the perpendicular current, causing the peak at $\theta = 0^\circ$. When the field is tilted, the flux lines penetrate the SC layers and then are strongly pinned in the SC layers, leading to a resistance decrease. As the field is further tilted, the SC state becomes unstable, which reduces the pinning force of the PVs. Therefore, the resistance should increase again. The overall behavior is explained by the above simple picture except the presence of the side peaks. Similar side peaks have been already observed in other 2D superconductors, λ-$(BETS)_2FeCl_4$ [16], λ-$(BETS)_2GaCl_4$ [13], κ-$(BEDT\text{-}TTF)_2Cu(NCS)_2$ [17], and a high T_c cuprate [18,19]. The side peaks may suggest a phase transition of the flux lines, likely a decoupling of the layers, but the origin is still controversial.

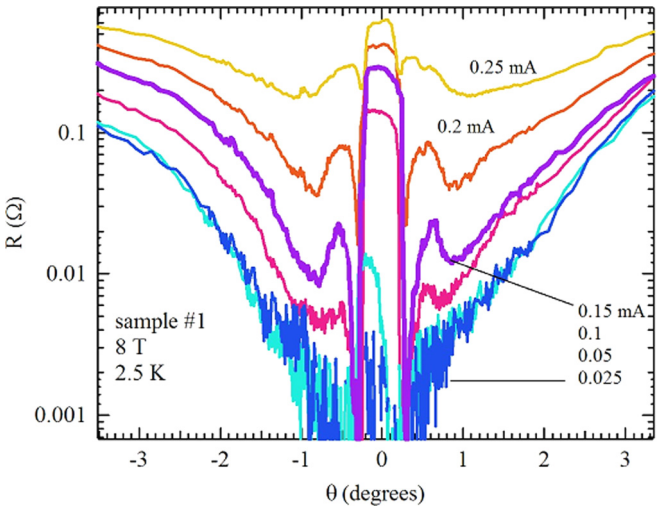

FIG. 5. Interlayer resistance ($I \parallel b^*$) as a function of the field angle θ at various currents for no. 1. The peak for $\theta = 0^\circ$ arises from the JV dynamics. The arrows indicate the side peaks.

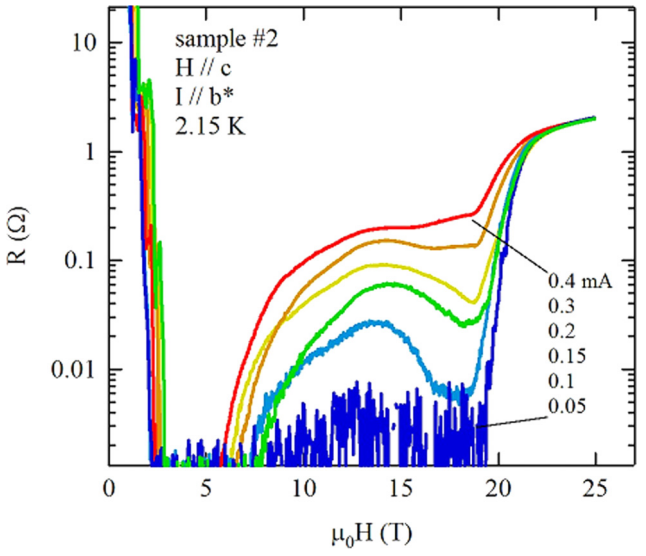

FIG. 6. Interlayer resistance as a function of the field for $H \parallel c$ at 2.15 K.

Figure 6 presents the interlayer resistance as a function of the field for $H \parallel c$ at 2.15 K. At the lowest current, (0.05 mA), the resistance drastically decreases to zero at ∼3 T with increasing field (AFI-SC transition). After that, the resistance remains below the noise level up to ∼19 T and then rapidly increases to the normal state value above ∼23 T. At higher currents, we note that the resistance is significantly enhanced below 20 T, due to the JV dynamics. A resistance maximum is seen at ∼14 T. Above 23 T, the resistance is independent of current, suggesting $H_{c2} \simeq 23$ T.

Figure 7 presents the interlayer resistance as a function of the field at various field angles for the current of 0.15 mA. For $\theta = 0^\circ$, the resistance has a broad maximum at ∼14 T. As the field is tilted, the flux lines are pinned in the SC layers, leading to the reduction of the resistance. For $\theta = 0.4^\circ$, the broad maximum completely disappears and the resistance becomes below the noise level in a wide field region between 2.5 T and 15 T. As the field is further tilted, H_{c2} is reduced and the $R(H)$

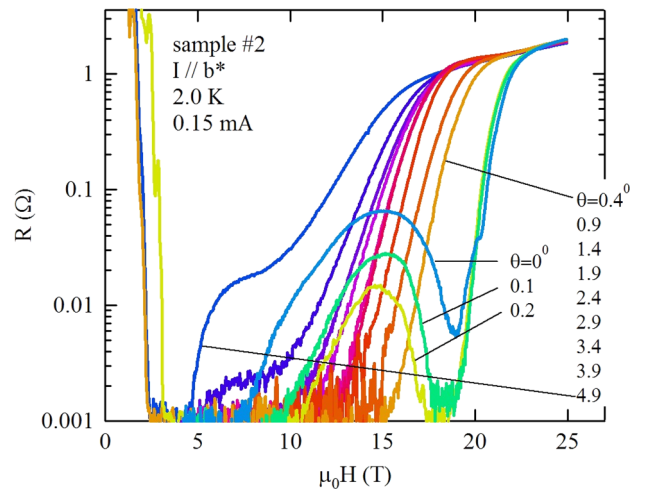

FIG. 7. Interlayer resistance as a function of the field at various field angles for 0.15 mA. The current 0.1 mA corresponds to 0.5 A/cm^2.

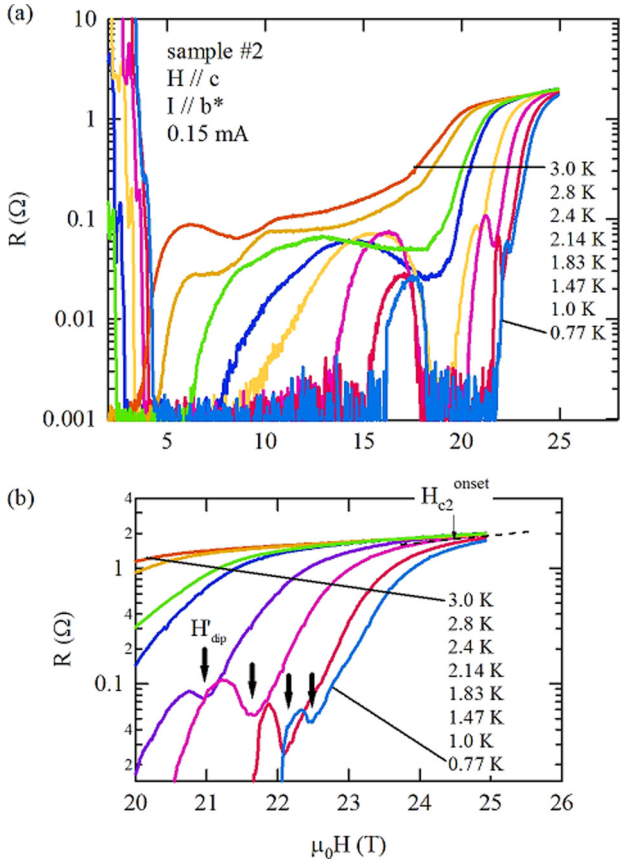

FIG. 8. (a) Interlayer resistance as a function of the field at various temperatures for the current of 0.15 mA. (b) Closeup of the high field region.

curve simply shifts to a low field region. The results in Figs. 6 and 7 clearly show that the JVs dynamics lead to the broad resistance maximum at ∼14 T.

Figure 8(a) presents the interlayer resistance as a function of the field at various temperatures for the current of 0.15 mA. At 0.77 K, the resistance is below the noise level in a wide field region but a broad peak is observed at 17 T. As temperature increases, the peak shifts to a low field and becomes broader. At 3.0 K, the zero resistance is observed only in a limited region below 3 T. A significant feature is that a small dip in addition to the broad peak is observed above 20 T as indicated by arrows in Fig. 8(b). The small dip field $H'_{\rm dip}$ decreases with increasing temperature and disappears above ∼2 K.

Figure 9 presents the temperature-field phase diagram for $H \parallel c$, where $T_c^{\rm onset}$, $T_{\rm SI}$, and $T_{\rm dip}$ obtained from $R(T)$ curves for no. 1, and $H_{c2}^{\rm onset}$, $H_{\rm SI}$, and $H'_{\rm dip}$ from $R(H)$ curves for no. 2 are plotted.

B. Magnetic torque

The magnetic torque τ is defined as $\tau = \mu_0 \mathbf{M} \times \mathbf{H}$, where $\mathbf{M}$ is the magnetization. For highly 2D superconductors, when the in-plane field H_x is much larger than the in-plane lower critical field, the magnetic torque is written as $\tau \simeq \mu_0 M_z H_x$ [20], where M_z is the perpendicular diamagnetism. Therefore, τ/H_x vs H_z plot gives the magnetization curve $M_z(H_z)$.

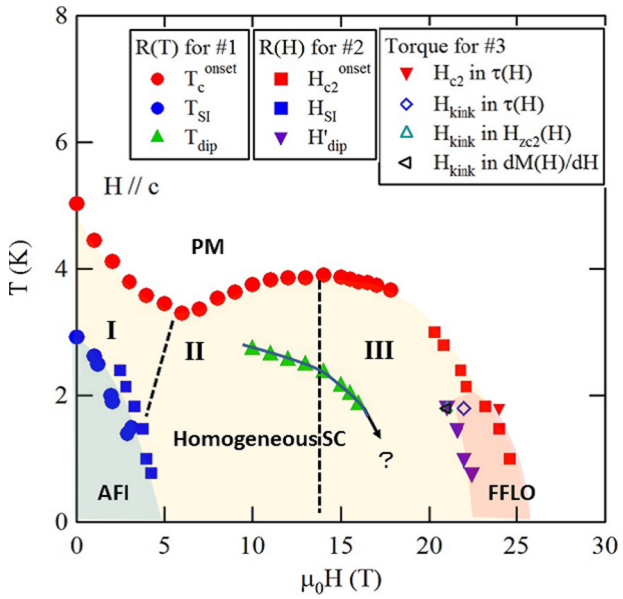

FIG. 9. Temperature-field phase diagram for $H \parallel c$. T_c^{onset}, T_{SI}, and T_{dip} are obtained from $R(T)$ curves for no. 1. H_{c2}^{onset}, H_{SI}, and H_{dip} are from $R(H)$ curves for no. 2. H_{c2}^{onset} and H_{kink} are from the torque data of no. 3.

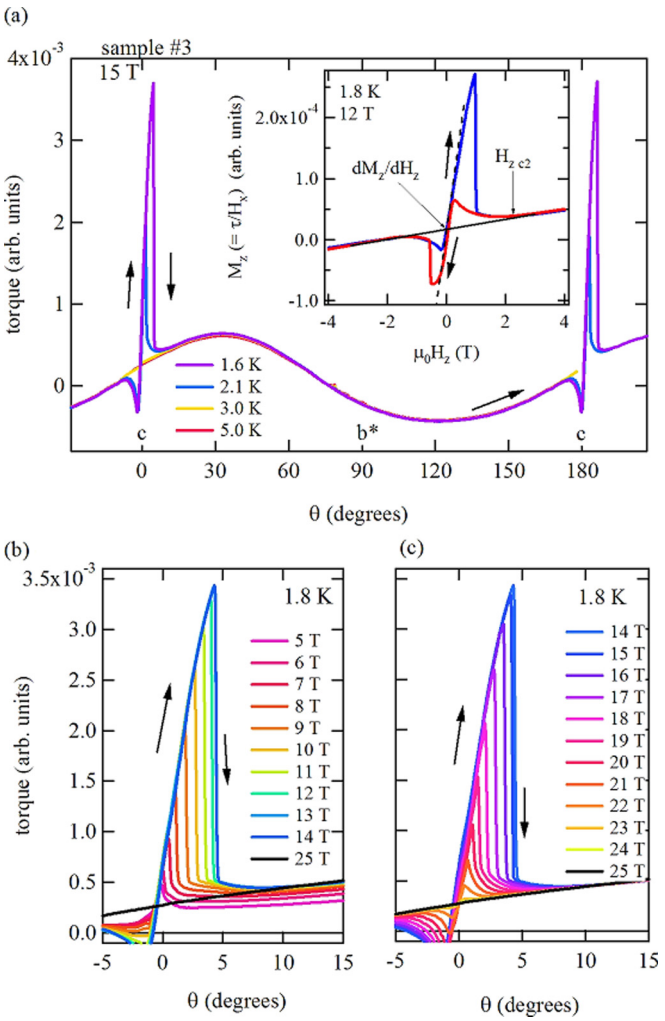

FIG. 10. (a) Torque curves as a function of the magnetic field angle θ at various temperatures. Inset: $M_z(H_z)$ curves calculated from the torque curves at 1.8 K. A black solid curve is the background arising from the $3d$ spins. The dotted line indicates the slope at $H_z \to 0$. The perpendicular critical field H_{zc2} is defined as shown by the thin arrow. Closeups of the torque curves at (b) low and (c) high fields.

Figure 10(a) presents typical torque curves as a function of the magnetic field angle θ at various temperatures. Above T_c, we observe only a sinusoidal torque curve, arising from the localized $3d$ spins. Sharp features for $\theta \simeq 0^\circ$ and 180° are caused by the SC transition. In this way, one of the advantages of the torque measurements is that we can clearly separate the background and SC signal from the raw data. The asymmetric torque signals around $\theta = 0^\circ$ and 180° are due to a nonlinear effect of the cantilever. The inset shows the $M_z(H_z)$ curves calculated from the torque curves. Since the flux lines are pinned in the SC layers, the M_z curves show large hysteresis.

In parallel fields ($\theta = 0^\circ$), all the flux lines penetrate the insulating layers ($M \parallel H$) and the π electrons show no torque; $M_z = 0$. The diamagnetic signal steeply increases as the field is tilted from the layers. The almost linear relation, $M_z \propto H_z$ at $\theta \simeq 0$, means that most of the flux lines remain in the insulating layers but do not penetrate the SC layers; most of the flux lines are pinned at the sample edges. As the magnetic field is tilted, M_z has a sudden decrease, showing that many flux lines are depinned and start penetrating in the SC layers (the flux lines are depinned) [21]. At the higher angles, the M_z curves become reversible and then the SC state is completely broken ($M_z = 0$), where we can define the perpendicular critical field H_{zc2}. The slope of the M_z curve at $\theta = 0^\circ$ corresponds to the diamagnetic susceptibility dM_z/dH_z in the low field limit ($H_z \to 0$). Figures 10(b) and 10(c) present the closeups of the torque curves at low and high fields, respectively.

Figure 11(a) presents the field dependences of the background torque arising from the $3d$ spins τ_{3d} and the peak of the torque curve τ_{peak}, which are defined in the inset. The τ_{3d} value steeply increases with field and has a tendency to saturate above 7 T, showing that H_{int} is saturated.

By contrast, the torque peak τ_{peak} due to the SC transition has a maximum at 14 T. The maximum shows that the PVs are pinned most strongly in the SC layers. Figures 11(b) and 11(c) present H_{zc2} and $-dM_z/dH_z$ as a function of field at 1.8 K, respectively. The H_{zc2} value has a maximum at ~15 T and then steeply decreases above 21 T, where a kink is evident. The maximum of H_{zc2} at ~15 T is consistent with the maximum of T_c at ~14 T, showing that the superconductivity is most stable. The $-dM_z/dH_z$ value gradually decreases with increasing field and then shows a similar kink at ~21 T. The kinks in the H_{zc2} and $-dM_z/dH_z$ data suggest a phase transition as discussed later.

Figure 12(a) shows the field dependence of the magnetic torque at various field angles. All the torque curves show a sharp feature at ~1.5 T, probably arising from the spin-flop transition. The AFI-SC transition should be present at ~3 T, but no significant anomaly is evident. Each torque curve exhibits hysteresis between the up and down field sweeps. The hysteresis shows the flux line pinning, which is a clear

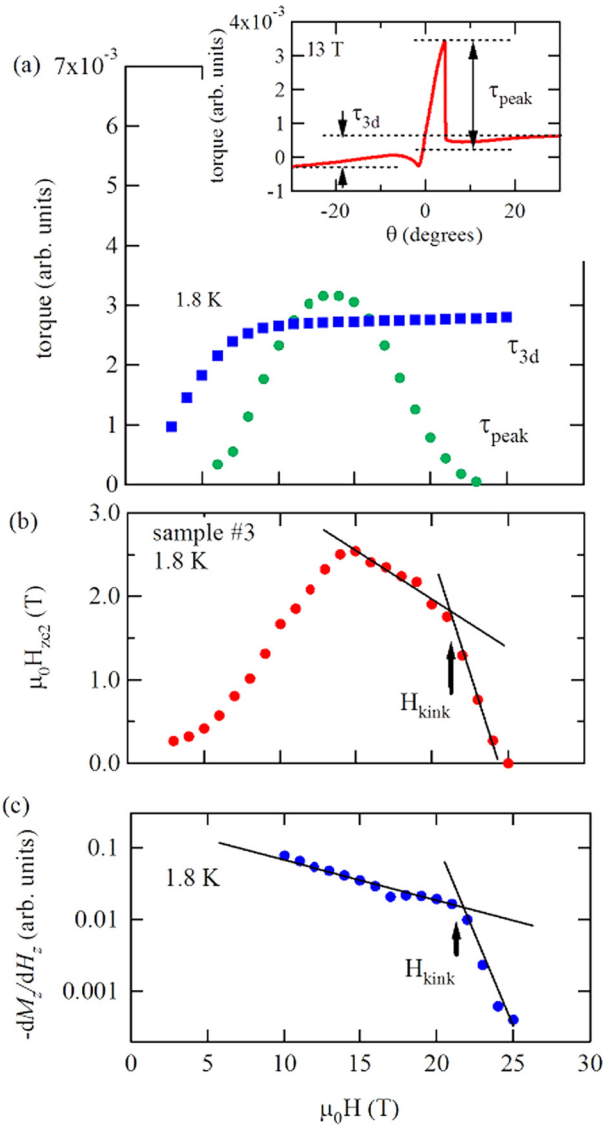

FIG. 11. (a) Torque of the $3d$ spin τ_{3d} and peak height of the torque curve τ_{peak}. Inset: definitions of τ_{3d} and τ_{peak}. (b) Perpendicular critical field H_{zc2}. (c) Diamagnetic susceptibility $-M_z(H_z)$ for $H_z \to 0$. The kinks are indicted by arrows in (b) and (c).

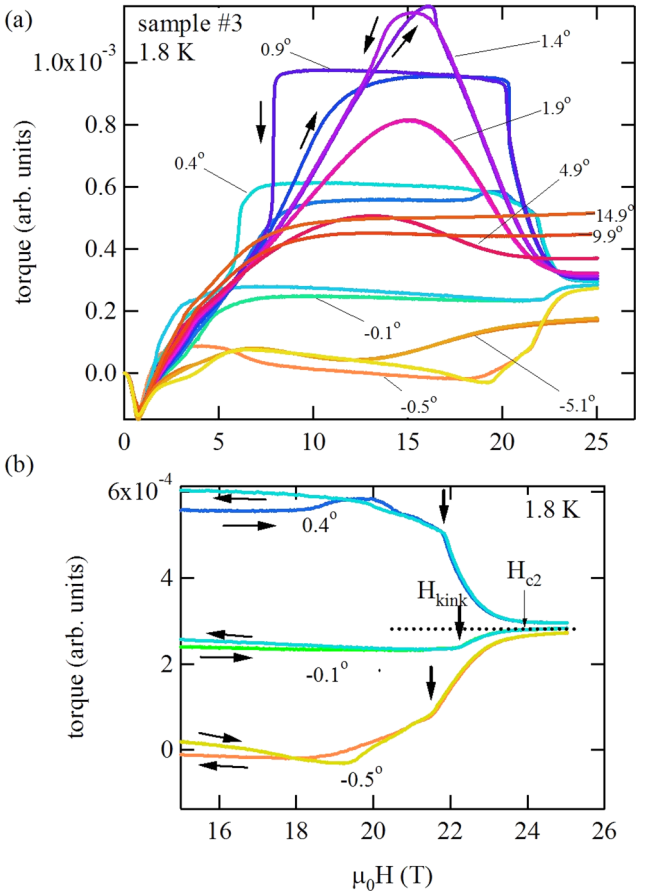

FIG. 12. (a) Field dependences of the torque as function of field at various angles. (b) Closeup of the high field torque data. Thick arrows indicate kinks.

sign of the bulk superconductivity (not SC fluctuation). We see that some torque curves are undulating in the wide field region. When the field is tilted, the flux lines penetrate in the SC layers and form complicated structures made of the JVs and PVs, depending on temperature and field [22–24]. Such structures may lead to various torque anomalies with field as observed in Fig. 12(a). We see a broad maximum at ∼15 T for $1.4^\circ \leqslant \theta \leqslant 4.9^\circ$. For $\theta \geqslant 9.9^\circ$, the SC does not appear and only a monotonic increase is observed above ∼1.5 T. This field dependence is consistent with the $\tau_{3d}(H)$ curve in Fig. 11(a). An interesting feature is seen for $\theta \approx 0^\circ$ as shown in Fig. 12(b). Each torque curve has hysteresis up to ∼22 T and then a kink (thick arrow) appears. This kink field H_{kink} agrees with those obtained from the results in Fig. 11. After the kink, the torque becomes completely reversible and then almost independent of field, where we can define H_{c2}. This H_{c2} value also agrees with the onset field H_{c2}^{onset} of the resistive transition [Fig. 8(b)]. The kink is absent for $\theta > 0.9^\circ$. The H_{kink} and H_{c2} values are also plotted in Fig. 9.

IV. DISCUSSION

A. Phase diagram and JV dynamics

In Fig. 9, the SC phase can be divided into three vortex phases, I, II, and III. Phases I and III are diamagnetic ($M_\pi < 0$) vortex phases where $H_{int} < H$. Phase II is a paramagnetic ($M_\pi > 0$) vortex phase ($H_{int} > H$). According to Eqs. (3) and (5), both j_p and M_π vanish at the boundaries (dashed lines) in the phase diagram, where $H = H_{int}$.

Figure 13 presents schematic pictures of (a) a JV in the layer structure and its supercurrent $j_s(r)$ for $H \parallel$ layer, and (b) the spin polarization current $j_p(r)$. The Fe or Ga anions are indicated by blue circles. Because of the large anisotropy of the coherence length, the JV is strongly elongated in the layer direction and, consequently, the supercurrent j_s around the JV spreads over a wide range, which is wider than the in-plane coherence length ∼10 nm [14]. On the other hand, the π-d interaction, which is a very short range interaction, will induce H_J and j_p only in the range of a few BETS molecules. All the values, H_J, j_s, and j_p are very inhomogeneous microscopically. Therefore, M_π and j_p cannot vanish locally even for $H = H_{int}$. The essential point will be

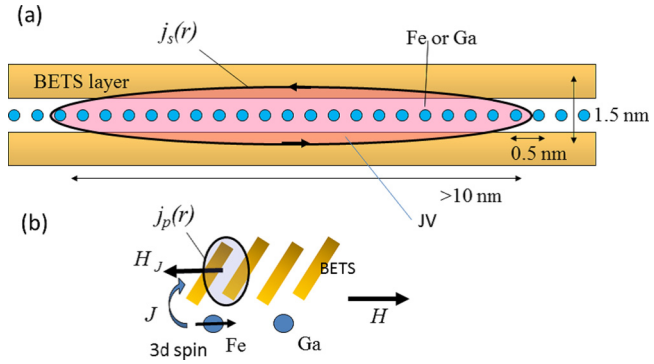

FIG. 13. Schematic pictures of (a) a JV in the layer structure and its supercurrent $j_s(r)$ and (b) the spin polarization current $j_p(r)$.

that the perpendicular external current I drives only the JVs accompanied by j_s, which originates from the orbital effect of the field, and then induces the voltage $V \propto N_{\rm JV} v_{\rm JV} \Phi_0$ in the interlayer direction.

The T_c value has a maximum at ~14 T, showing that the order parameter $|\Psi(r)|$ in the SC layers has a maximum. It suggests that the PVs are pinned most strongly at the sample edges at ~14 T, which is consistent with the $\tau_{\rm peak}$ maximum in Fig. 11(a). However, the resistance surprisingly has a broad maximum at ~14 T in Fig. 6, showing that the JVs are driven most easily ($N_{\rm JV} v_{\rm JV}$ is the largest). This finding provides a sharp contrast to the results in an isostructural superconductor λ-$(BETS)_2GaCl_4$ [13], where the finite resistance due to the JV dynamics is observed only near H_{c2} (the JVs cannot be driven at low fields). The difference can be ascribed to H_J inducing the spin polarization current j_p, although the microscopic origin is not clear.

The temperature dependence of the resistance in fields has the dip (Fig. 2), whose temperature ($T_{\rm dip}$) is indicated by green triangles in Fig. 9. The presence of the dip suggests a JV transition. The JV phase diagram in highly 2D superconductors has been investigated by Monte Carlo simulations based on an anisotropic frustrated XY model [25,26]. The results show that the JVs at low temperatures are decoupled between the layers although the JV lattice is kept in each layer as field increases. At high temperatures, the JV lattice melts and a JV liquid phase appears. The resistance dip in Fig. 2 may be related to the decoupling between the layers but we have not obtained any evidence of a melting transition of the JVs in the torque data. Further investigation is required to understand the origin of the dip.

B. FFLO phase boundary

In parallel field for layered superconductors, the orbital effect is quenched and thus the Zeeman effect predominantly governs the superconductivity, which gives the paramagnetic (Pauli) limit, $H_{\rm Pauli}$. In the weak coupling BCS model, we obtain $H_{\rm Pauli} = 1.84 T_c$ [T/K]. In conventional superconductors, the SC order parameter is spatially homogeneous. However, when the superconductivity is in the clean limit and the orbital effect is quenched, an inhomogeneous SC state where the order parameter oscillates in real space can be stabilized even above $H_{\rm Pauli}$. This state was first proposed by Fulde and Ferrell [27] and Larkin and Ovchinnikov (FFLO) [28]. So far, extensive efforts have been made to discover the presence of the FFLO phase in strongly correlated electron systems [29–31] and in organic superconductors [32–39].

In λ-$(BETS)_2FeCl_4$ ($x = 1.0$), a FFLO phase in the FISC phase has been investigated theoretically [40,41] and experimentally [7,13,16,21,42]. The interlayer resistance shows successive dips in parallel field for $H_{c2} < H < 25$ T. The dips are interpreted as the magnetic field-dependent commensurability effect between the spatially varying wavelength of the FFLO order parameter and the JV lattice constant [42,43]: the dips appear when the JV lattice is collectively pinned by the nodes of the FFLO order parameter. The steep decrease of the diamagnetic susceptibility $-dM_z/dH_z$ is found at ~25 T, which is consistent with the nodal structure of the order parameter in the FFLO phase. For λ-$(BETS)_2GaCl_4$ ($x = 0$), on the other hand, such commensurability effect is not observed in the resistive transition [13]. However, the steep decreases of $-dM_z/dH_z$ and the JV depinning current are found at ~10 T, showing a FFLO transition. For both salts, all these anomalies are observed only at low temperatures, $T < 0.5T_c$, and disappear when the field is tilted from the c axis by a few degrees. In κ-$(BEDT\text{-}TTF)_2Cu(NCS)_2$, a similar reduction of $-dM_z/dH_z$ is also observed at ~21 T [39], which is ascribed to a FFLO transition.

For λ-$(BETS)_2Fe_{1-x}Ga_xCl_4$ ($x = 0.37$), we have presented some anomalies showing a phase transition at ~22 T in the SC phase (Fig. 9), the dips in the $R(H)$ curves, and kinks in the $\tau(H)$, H_{zc2}, and dM/dH curves. These features strongly suggest the FFLO transition at ~22 T. Taking $T_c = 5$ K, we obtain $H_{\rm Pauli} = 1.84T_c \simeq 9$ T. Since $H_{\rm int} = 14$ T, we may have the FFLO transition at ~23 T, which is close to $H_{\rm dip}$ and $H_{\rm kink}$. The dip in the $R(H)$ curve and the kink in the $\tau(H)$ curve disappear when the field is slightly tilted from the c axis, which is also consistent with the FFLO phase. In both λ-$(BETS)_2FeCl_4$ and λ-$(BETS)_2GaCl_4$, the FFLO transition fields also agree with the calculated $H_{\rm Pauli}$ [13,16,21,42].

For all these salts ($x = 1.0, 0.37$, and 0), as discussed above, the significant signs of the FFLO phase transition have been obtained. However, different behavior is found in the resistive transitions; successive dips for $x = 1.0$, a dip for $x = 0.37$, and no dip for $x = 0$. An important difference among these salts is the two dimensionality of the superconductivity, whose good measure is the orbital critical field H_{c2}^* in parallel fields. The phase diagram analyses [14] show that H_{c2}^* increases with increasing x; the superconductivity becomes more 2D with increasing x. Therefore, the JVs are pinned more weakly with increasing x. which enables us to observe the JV dynamics more easily.

V. SUMMARIES

The interlayer resistance and magnetic torque measurements have been performed in a wide temperature and field range for λ-$(BETS)_2Fe_{1-x}Ga_xCl_4$ ($x = 0.37$). The phase diagram for $H \parallel$ layer is found to have the maximum T_c at 14 T, showing the presence of the internal field $H_{\rm int} = 14$ T by the localized $3d$ spins of the Fe ions. The simple GL analyses predict that the diamagnetic signal of the conduction π electrons, M_π, vanishes at 14 T in the superconducting

phase, where no conventional vortices are formed. However, we observe large energy dissipation of the JVs in the wide temperature and field region. The results show that the perpendicular current I drives only the JVs accompanied by the supercurrent j_s, arising from the orbital effect. The strongest energy dissipation of the JVs at ∼14 T shows the weakest pinning force of the JVs. It is likely related to the microscopic distribution of j_p. The τ_{peak} maximum (the largest pinning of the PVs at the sample edges) is observed at ∼14 T, which is consistent with the T_c (the order parameter) maximum. The interlayer resistance in parallel fields shows a characteristic dip with decreasing temperature, suggesting a JV transition. At ∼23 T, we can observe some signs of an inhomogeneous (FFLO) superconducting transition.

ACKNOWLEDGMENT

This work was supported by a Grant-in-Aid for Scientific Research from MEXT (Grant No. 25400384).

[1] H. Kobayashi, H. Tomita, T. Naito, A. Kobayashi, F. Sakai, T. Watanabe, and P. Cassoux, J. Am. Chem. Soc. **118**, 368 (1996).
[2] L. K. Montgomery, T. Burgin, J. C. Huffman, J. Ren, and M.-H. Whangbo, Physica C **219**, 490 (1994).
[3] L. Brossard, R. Clerac, C. Coulon, M. Tokumoto, T. Ziman, D. K. Petrov, V. N. Laukhin, M. J. Naughton, A. Audouard, F. Goze, A. Kobayashi, H. Kobayashi, and P. Cassoux, Eur. Phys. J. B **1**, 439 (1998).
[4] H. Akiba, K. Nobori, K. Shimada, Y. Nishio, K. Kajita, B. Zhou, A. Kobayashi, and H. Kobayashi, J. Phys. Soc. Jpn. **80**, 063601 (2011); H. Akiba, H. Sugawara, K. Nobori, K. Shimada, N. Tajima, Y. Nishio, K. Kajita, B. Zhou, A. Kobayashi, and H. Kobayashi, *ibid.* **81**, 053601 (2012).
[5] S. Sugiura, K. Shimada, N. Tajima, Y. Nishio, T. Terashima, T. Isono, A. Kobayashi, B. Zhou, R. Kato, and S. Uji, J. Phys. Soc. Jpn. **85**, 064703 (2016); S. Sugiura, K. Shimada, N. Tajima, Y. Nishio, T. Terashima, T. Isono, R. Kato, and S. Uji, *ibid.* **86**, 014702 (2017).
[6] S. Uji, H. Shinagawa, T. Terashima, T. Yakabe, Y. Terai, M. Tokumoto, A. Kobayashi, H. Tanaka, and H. Kobayashi, Nature (London) **410**, 908 (2001).
[7] L. Balicas, J. S. Brooks, K. Storr, S. Uji, M. Tokumoto, H. Tanaka, H. Kobayashi, A. Kobayashi, V. Barzykin, and L. P. Gorkov, Phys. Rev. Lett. **87**, 067002 (2001).
[8] S. Uji, H. Shinagawa, C. Terakura, T. Terashima, T. Yakabe, Y. Terai, M. Tokumoto, A. Kobayashi, H. Tanaka, and H. Kobayashi, Phys. Rev. B **64**, 024531 (2001); S. Uji, C. Terakura, T. Terashima, T. Yakabe, Y. Terai, M. Tokumoto, A. Kobayashi, F. Sakai, H. Tanaka, and H. Kobayashi, *ibid.* **65**, 113101 (2002).
[9] V. Jaccarino and M. Peter, Phys. Rev. Lett. **9**, 290 (1962).
[10] O. Fischer, Helv. Phys. Acta **45**, 331 (1972).
[11] K. Hiraki, H. Mayaffre, M. Horvatic, C. Berthier, S. Uji, T. Yamaguchi, H. Tanaka, A. Kobayashi, H. Kobayashi, and T. Takahashi, J. Phys. Soc. Jpn. **76**, 124708 (2007).
[12] C. Mielke, J. Singleton, M.-S. Nam, N. Harrison, C. C. Agosta, B. Fravel, and L. K. Montgomery, J. Phys.: Condens. Matter **13**, 8325 (2001).
[13] S. Uji, K. Kodama, K. Sugii, T. Terashima, T. Yamaguchi, N. Kurita, S. Tsuchiya, T. Konoike, M. Kimata, A. Kobayashi, B. Zhou, and H. Kobayashi, J. Phys. Soc. Jpn. **84**, 104709 (2015).
[14] S. Uji, T. Terashima, C. Terakura, T. Yakabe, Y. Terai, S. Yasuzuka, Y. Imanaka, M. Tokumoto, A. Kobayashi, F. Sakai, H. Tanaka, H. Kobayashi, L. Ballicas, and J. S. Brooks, J. Phys. Soc. Jpn. **72**, 369 (2003); S. Uji and J. S. Brooks, *ibid.* **75**, 051014 (2006).
[15] O. Fischer, H. W. Meul, M. G. Karkut, G. Remenyi, U. Welp, J. C. Piccoche, and K. Maki, Phys. Rev. Lett. **55**, 2972 (1985).
[16] S. Uji, K. Kodama, K. Sugii, T. Terashima, T. Yamaguchi, N. Kurita, S. Tsuchiya, M. Kimata, T. Konoike, A. Kobayashi, B. Zhou, and H. Kobayashi, J. Phys. Soc. Jpn. **82**, 034715 (2013).
[17] S. Yasuzuka, S. Uji, H. Satsukawa, M. Kimata, T. Terashima, K. Koga, Y. Yamaura, K. Saito, H. Akutsu, and J. Yamada, Physica B **405**, S288 (2010); S. Yasuzuka, K. Saito, S. Uji, M. Kimata, H. Satsukawa, T. Terashima, and J. Yamada, J. Phys. Soc. Jpn. **82**, 064716 (2013); S. Yasuzuka, S. Uji, T. Terashima, S. Tsuchiya, B. Zhou, A. Kobayashi, and H. Kobayashi, *ibid.* **83**, 013705 (2014).
[18] M. Chaparala, O. H. Chung, Z. F. Ren, M. White, P. Coppens, J. H. Wang, A. P. Hope, and M. J. Naughton, Phys. Rev. B **53**, 5818 (1996).
[19] G. S. Okram, H. Aoki, M. Xu, D. G. Hinks, and T. W. Li, Solid State Commun. **118**, 47 (2001).
[20] J. C. Martinez, S. H. Brongersma, A. Koshelev, B. Ivlev, P. H. Kes, R. P. Griessen, D. G. de Groot, Z. Tarnavski, and A. A. Menovsky, Phys. Rev. Lett. **69**, 2276 (1992).
[21] S. Uji, K. Kodama, K. Sugii, T. Terashima, Y. Takahide, N. Kurita, S. Tsuchiya, M. Kimata, A. Kobayashi, B. Zhou, and H. Kobayashi, Phys. Rev. B **85**, 174530 (2012).
[22] L. N. Bulaevskii, M. Ledvij, and V. G. Kogan, Phys. Rev. B **46**, 366 (1992).
[23] A. E. Koshelev, Phys. Rev. Lett. **83**, 187 (1999); Phys. Rev. B **68**, 094520 (2003).
[24] G. Blatter, M. V. Feigel'man, V. B. Geshkenbein, A. I. Larkin, and V. M. Vinokur, Rev. Mod. Phys. **66**, 1125 (1994).
[25] X. Hu and M. Tachiki, Phys. Rev. B **70**, 064506 (2004); X. Hu, M. Luo, and Y. Ma, *ibid.* **72**, 174503 (2005).
[26] Y. Nonomura and X. Hu, Phys. Rev. B **74**, 024504 (2006).
[27] P. Fulde and R. A. Ferrell, Phys. Rev. **135**, A550 (1964).
[28] A. I. Larkin and Y. N. Ovchinnikov, Sov. Phys. JETP **20**, 762 (1974).
[29] F. Steglich, R. Modler, P. Gegenwart, M. Deppe, M. Weiden, M. Lang, C. Geibel, T. Liihmann, C. Paulsen, J. L. Tholence, Y. Onuki, M. Tachiki, and S. Takahashi, Physica C **263**, 498 (1996).
[30] H. A. Radovan, N. A. Fortune, T. P. Murphy, S. T. Hannahs, E. C. Palm, S. W. Tozer, and D. Hall, Nature (London) **425**, 51 (2003).
[31] A. Bianchi, R. Movshovich, C. Capan, P. G. Pagliuso, and J. L. Sarrao, Phys. Rev. Lett. **91**, 187004 (2003).
[32] J. Singleton, J. A. Symington, M-S. Nam, A. Ardavan, M. Kurmoo, and P. Day, J. Phys.: Condens. Matter **12**, L641 (2000).
[33] M. A. Tanatar, T. Ishiguro, H. Tanaka, and H. Kobayashi, Phys. Rev. B **66**, 134503 (2002).

[34] R. Lortz, Y. Wang, A. Demuer, P. H. M. Bottger, B. Bergk, G. Zwicknagl, Y. Nakazawa, and J. Wosnitza, Phys. Rev. Lett. **99**, 187002 (2007).
[35] K. Cho, B. E. Smith, W. A. Coniglio, L. E. Winter, C. C. Agosta, and J. A. Schlueter, Phys. Rev. B **79**, 220507 (2009).
[36] W. A. Coniglio, L. E. Winter, K. Cho, C. C. Agosta, B. Fravel, and L. K. Montgomery, Phys. Rev. B **83**, 224507 (2011).
[37] B. Bergk, A. Demuer, I. Sheikin, Y. Wang, J. Wosnitza, Y. Nakazawa, and R. Lortz, Phys. Rev. B **83**, 064506 (2011).
[38] J. A. Wright, E. Green, P. Kuhns, A. Reyes, J. Brooks, J. Schlueter, R. Kato, H. Yamamoto, M. Kobayashi, and S. E. Brown, Phys. Rev. Lett. **107**, 087002 (2011).
[39] S. Tsuchiya, J. Yamada, K. Sugii, D. Graf, J. S. Brooks, T. Terashima, and S. Uji, J. Phys. Soc. Jpn. **84**, 034703 (2015).
[40] M. Houzet, A. Buzdin, L. Bulaevskii, and M. Maley, Phys. Rev. Lett. **88**, 227001 (2002).
[41] H. Shimahara, J. Phys. Soc. Jpn. **71**, 1644 (2002).
[42] S. Uji, T. Terashima, M. Nishimura, Y. Takahide, T. Konoike, K. Enomoto, H. Cui, H. Kobayashi, A. Kobayashi, H. Tanaka, M. Tokumoto, E. S. Choi, T. Tokumoto, D. Graf, and J. S. Brooks, Phys. Rev. Lett. **97**, 157001 (2006).
[43] L. Bulaevskii, A. Buzdin, and M. Maley, Phys. Rev. Lett. **90**, 067003 (2003).